

Hand-Injectable Acrylic Bone Cement Applicator for Skull Base Bone Replacement

BEE 4530 – Computer Aided Engineering: Applications to Biomedical Processes

James Gonos
Mark Levatich
Ryan Smith
Corinne Zappacosta

Table of Contents

1.0 Executive Summary.....	1
2.0 Introduction.....	2
2.1 <i>Background</i>	
2.2 <i>Design Objectives</i>	
2.3 <i>Problem Schematic</i>	
3.0 Results and Discussion.....	8
3.1 <i>Qualitative Description of Process</i>	
3.2 <i>Sensitivity Analysis</i>	
3.3 <i>Accuracy Check</i>	
4.0 Conclusions and Design Recommendations.....	14
4.1 <i>Review of Objectives</i>	
4.2 <i>Realistic Constraints</i>	
5.0 Appendix A: Mathematical Statement of Problem.....	16
5.1 <i>Governing Equations</i>	
5.2 <i>Boundary and Initial Conditions</i>	
5.3 <i>Input Parameters</i>	
6.0 Appendix B: Solution Strategy.....	17
6.1 <i>Solver</i>	
6.2 <i>Mesh</i>	
6.3 <i>Mesh Convergence</i>	
7.0 Appendix C: Additional Visuals.....	20
8.0 Appendix D: References.....	23

Executive Summary

One of the only existing procedures to remove brain tumors at the skull base is endoscopic endonasal neurosurgery. The most difficult part of this surgery is closing the hole created in the skull, which currently is solved by stuffing fat and biocompatible foam in the hole and sealing it with glue. A better way of sealing this hole would be to use poly methyl methacrylate (PMMA) so that the hole is replaced with a material which more closely resembles bone. In order to better understand the delivery and application of PMMA bone cement into a patient's skull through the nasal passages by a surgeon, we modeled three-dimensional viscous fluid flow within a surgical device prototype. The model is comprised of a 5-mm diameter tube with a 1-mm diameter wire running through its center. This wire is secured in place with vertical and horizontal supports. We analyzed the effects of the supports and wire on velocity and pressure drop of PMMA material moving through the tube to see if there was any resistance created in the tube that would be unmanageable by an unaided surgeon. To model the fluid flow, we created a three dimensional geometric schematic of the device in COMSOL. We acquired material properties from related literature and ran multiple simulations with several mesh sizes with COMSOL using the 3-D incompressible Navier-Stokes steady state application mode. The overall goal of this project was to determine if a surgeon could push PMMA through the tube without assistance from machines. Using this model we could then determine the manual pressure needed to administer the PMMA into a patient's skull at an appropriate velocity. Our results indicated that the amount of applied pressure required would be 1.7 lbf, which is much less than the minimal value (~17 lbf) found in the literature regarding thumb strength.¹⁰ From simulations we obtained multiple velocity profiles and plots of pressure drop. Pressure decreases at a constant rate until the tube bends, the wire is introduced, or fluid passes by an obstruction at each point drop in pressure increases. The total amount of pressure drop in the tube was found to be 380 kPa. As we increased inlet velocity, the required applied pressure increased significantly, but not to a magnitude that would be unbearable to a human thumb. The model also gives valuable insight on the effects of obstructions on continuous, viscous fluid flow in a narrow tube.

Keywords: Acrylic bone cement injector, Poly methylmethacrylate (PMMA), Endonasal Endoscopy

Introduction

Traditionally, tumors of the skull base have been managed by open skull bifrontal craniotomy techniques to perform full resections of the lesions.^{4,5} While these techniques have proven successful, they require prolonged retraction of the frontal lobes and potentially disfiguring transfacial approaches associated with high morbidity and perioperative stress on the patient.^{4,5} In contrast to these, an endonasal approach allows direct and minimally invasive midline access to the entire skull base and accompanying cisternal spaces without the need for brain retraction¹. Constant improvements in imaging and guidance systems have supported the growing prevalence of endonasal endoscopy for the surgical management of anterior, middle, and posterior skull base tumors, both primary and recurrent.^{1,5}

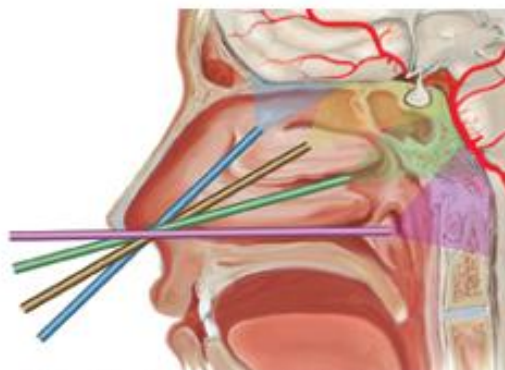


Fig. 1. Schematic drawing showing the different areas of the midline skull base exposed through the endoscopic endonasal approach. The various endoscopic trajectories are illustrated with different colors. Blue marks the endoscopic trajectory to the olfactory groove; yellow shows the trajectory to the sella turcica and planum sphenoidale; green marks the approach to the clivus; and purple shows the trajectory to the craniovertebral junction and foramen magnum.
Borrowed from Cavallo et al., p. 2.

One major drawback associated with this technique is the potential for intra and postoperative cerebrospinal fluid (CSF) leakage due to the required opening of the dura matter over the tuberculum sellae and posterior planum sphenoidale in accessing the skull base.¹ Persistent CSF leakage can lead to postural headache, pneumocephalus and, most importantly, meningitis infection.³

The current procedure for plugging the created fistula involves foam, muscle, and fatty tissue packing, skin grafts, and fibrin glue.³ In most cases, more than one fistula is present and the complete obliteration of the sinuses with similar packing is required.³ While effective, these procedures are manually difficult, often require multiple attempts to secure persistent leaks, and are undesirable to the patient.³

Acrylic bone cements, specifically poly methylmethacrylate (PMMA), have been successfully implemented in several orthopedic surgical procedures, notably percutaneous vertebroplasty² and anchorage for arthroplasties.^{8,9,11} PMMA bone cements are well-characterized, biocompatible, non-Newtonian pseudoplastics with increasing rates of viscosity with time.^{8,11} The device proposed in this project presents a user-friendly applicator for the direct delivery of the sealant PMMA bone cement to the problematic fistula immediately after surgery. The surgeon's hand-applied pressure on one end of the device forces the bone cement along the length of a cannula to exit into the fistula. The cannula is designed with a central rotating (churning) guide wire and accompanying supports running its length to assist with the accurate delivery of the viscous PMMA mixture.

Design Objective

The design requires that the cannula be small enough to penetrate the nasal cavity and sinuses while still allowing for the controlled flow of the viscous bone cement. The resistance produced by the acrylic bone cement as it is pushed through the thin applicator tube is a concern regarding the practicality of the proposed biomedical device. Specifically, we ask whether or not a surgeon could realistically force the bone cement through the device in a controllable manner, using their hand without mechanical assistance.

The high surface-to-volume ratio of the bone cement in the thin cannula combined with the frictional forces associated with the wire and support obstructions create the potential for the required pressure to exceed comfortable levels for the surgeon. This study aims to evaluate the pressure loss along the cannula to assess the feasibility of a hand-injector applicator for PMMA bone cement in endonasal endoscopy. To assess this feasibility, we sought to determine the pressure at the inlet of the tube, where the hand applies the pressure, provided a specified input velocity of the cement (discussed in *Problem Schematic*) and assuming the outlet pressure to be that of the sinuses (atmospheric pressure) using 3-D modeling in COMSOL. We then compared the corresponding pressure with published values of adduction pressures for males' thumbs.

Due to the limitations of our equipment's computational capacity coupled with our 3-D model, we modeled the cement's viscosity as Newtonian. Furthermore, our model employs a constant viscosity value. In order to address the reality of an increasing viscosity with time, several solutions were calculated based on different constant viscosity values in a sensitivity analysis.

Several considerations were taken into account for this model. Most importantly, different PMMA bone cements have varying rheological properties that depend on the preparative mixing method, time after initial mixing, and temperature.^{8,11} The application of bone cement in orthopedic surgeries typically occurs within 3-8 minutes of cement mixing which is considered right before rapid curing.^{6,8,9} We also assumed that the difference between room temperature and that inside the nasal cavity was negligible. Thus, for this project, viscosity values were taken from Lian et. al.'s experimentally-determined values for a low-viscosity bone cement, Simplex-P, at room temperature (25° Celsius), before the onset of rapid curing.⁶ This is shown by the linear region in Figure 2 on the next page.

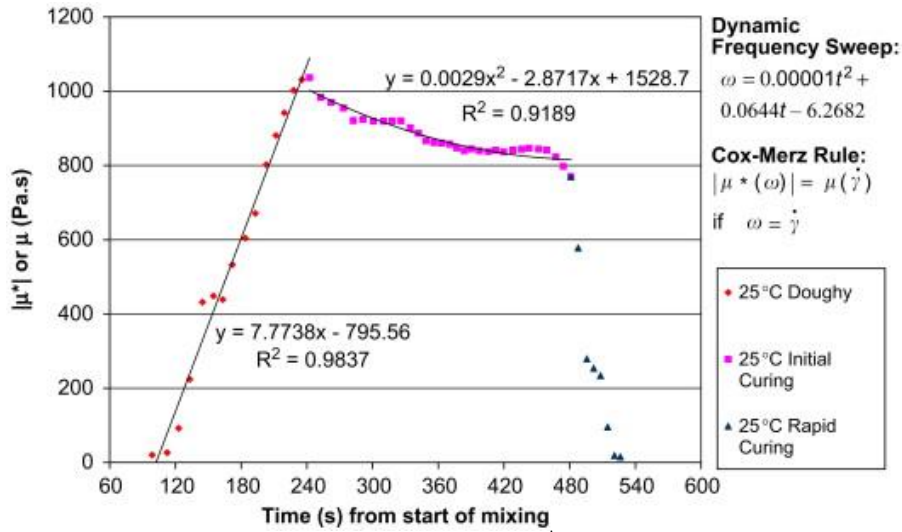


Figure 2. Bone cement complex-viscosity magnitude $|\mu^*|$ (or steady-state shear viscosity μ) against time from start of bone cement mixing at 25°C. The curve is derived from the experimental curve of $|\mu^*|$ against angular frequency ω in a dynamic frequency sweep at 25°C, which is mapped to time domain by applying the frequency variation $\omega(t)$ with time. The experimental points and fitted curves in this plot serve to reveal the three distinct phases of bone cement curing, namely the doughy, initial curing and rapid curing phases. – Lian et. al, 2007. The static value of 100 Pa·s was chosen because it is reasonably early in the curing process and in the range of time when a surgeon would be operating. This time span includes mixing the cement and filing the tube with cement to the tip before entering the sinuses. A single viscosity was chosen because the time of injection once in the sinuses would be no more than a couple seconds and the viscosity would change negligibly in that time span.

Problem Schematic

Governing Equations

The PMMA flow was modeled as non-compressible Newtonian fluid flow using steady-state Navier-Stokes equations in Cartesian coordinates in COMSOL.

$$\begin{aligned} \rho \left(u \frac{\partial u}{\partial x} + v \frac{\partial u}{\partial y} + w \frac{\partial u}{\partial z} \right) &= -\frac{\partial p}{\partial x} + \mu \left(\frac{\partial^2 u}{\partial x^2} + \frac{\partial^2 u}{\partial y^2} + \frac{\partial^2 u}{\partial z^2} \right) \\ \rho \left(u \frac{\partial v}{\partial x} + v \frac{\partial v}{\partial y} + w \frac{\partial v}{\partial z} \right) &= -\frac{\partial p}{\partial y} + \mu \left(\frac{\partial^2 v}{\partial x^2} + \frac{\partial^2 v}{\partial y^2} + \frac{\partial^2 v}{\partial z^2} \right) \\ \rho \left(u \frac{\partial w}{\partial x} + v \frac{\partial w}{\partial y} + w \frac{\partial w}{\partial z} \right) &= -\frac{\partial p}{\partial z} + \mu \left(\frac{\partial^2 w}{\partial x^2} + \frac{\partial^2 w}{\partial y^2} + \frac{\partial^2 w}{\partial z^2} \right) \end{aligned}$$

where ρ is density (kg/m^3), u is velocity in the x-direction (m/s), v is velocity in the y-direction (m/s), w is velocity in the z-direction (m/s), p is pressure (Pa), and μ is dynamic viscosity (Pa·s). Note that gravity was ignored due to reduce computational loads on available equipment

considering the negligible effect gravity would have on the relative pressure drop along the tube's length.

Schematic

The cannula with injector device was simplified to a hollow cylindrical tube with two bends of 150° (in opposite directions) in the tube as shown in Figure 3. The guide wire is isolated to the center of Section 3 of the tube, beginning at Bend 2 and terminating at the outlet (see Figure 3a).

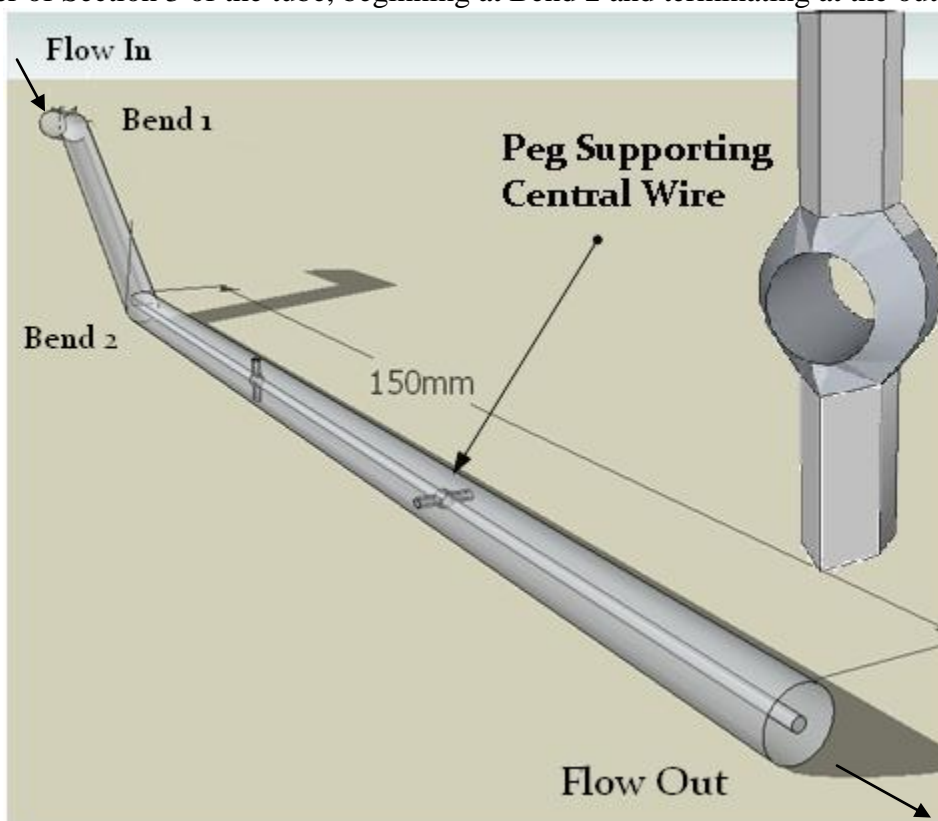


Figure 3. Cartoon model of tube of hand operated acrylic bone cement applicator. Section 1 of the tube is between the inlet and Bend 1; Section 2 is between Bend 1 and Bend 2; Section 3 is between Bend 2 and the outlet. An enlarged representation of one of the pegs that supports the guide wire which runs through the hole in the center of the peg is shown. Note that geometry of the peg is not cylindrical but consists of flat surfaces.

Boundary Conditions

Further simplifications were incorporated for the model used by COMSOL and are shown in Figure 4, along with the boundary conditions. Due to symmetry, only half of the tube was necessary for computations. Also, both of the two supporting pegs were oriented in the vertical, or z-axis, direction as shown in Figure 4a. Furthermore, the shape of the peg was simplified to a rectangular prism, oriented so that the vertices pointed in the positive and negative x-direction.

This is apparent by the v-shaped structure for half of the peg shown in Figure 4b. The boundary and initial conditions are depicted in Figure 4c.

- Outlet Pressure = 0 Pa
- Inlet Velocity = 7.13 mm/s
- No-slip boundaries at tube outer wall, tube-wire interfaces, and tube-peg interfaces.
- Symmetry boundary along central z-axis of tube.

The inlet velocity of 7.13 mm/s was based on an approximation of a 30-second application time through the ~200 mm path length (of the tube) for the PMMA. This approximation was based from direct observation of endonasal endoscopic procedures.

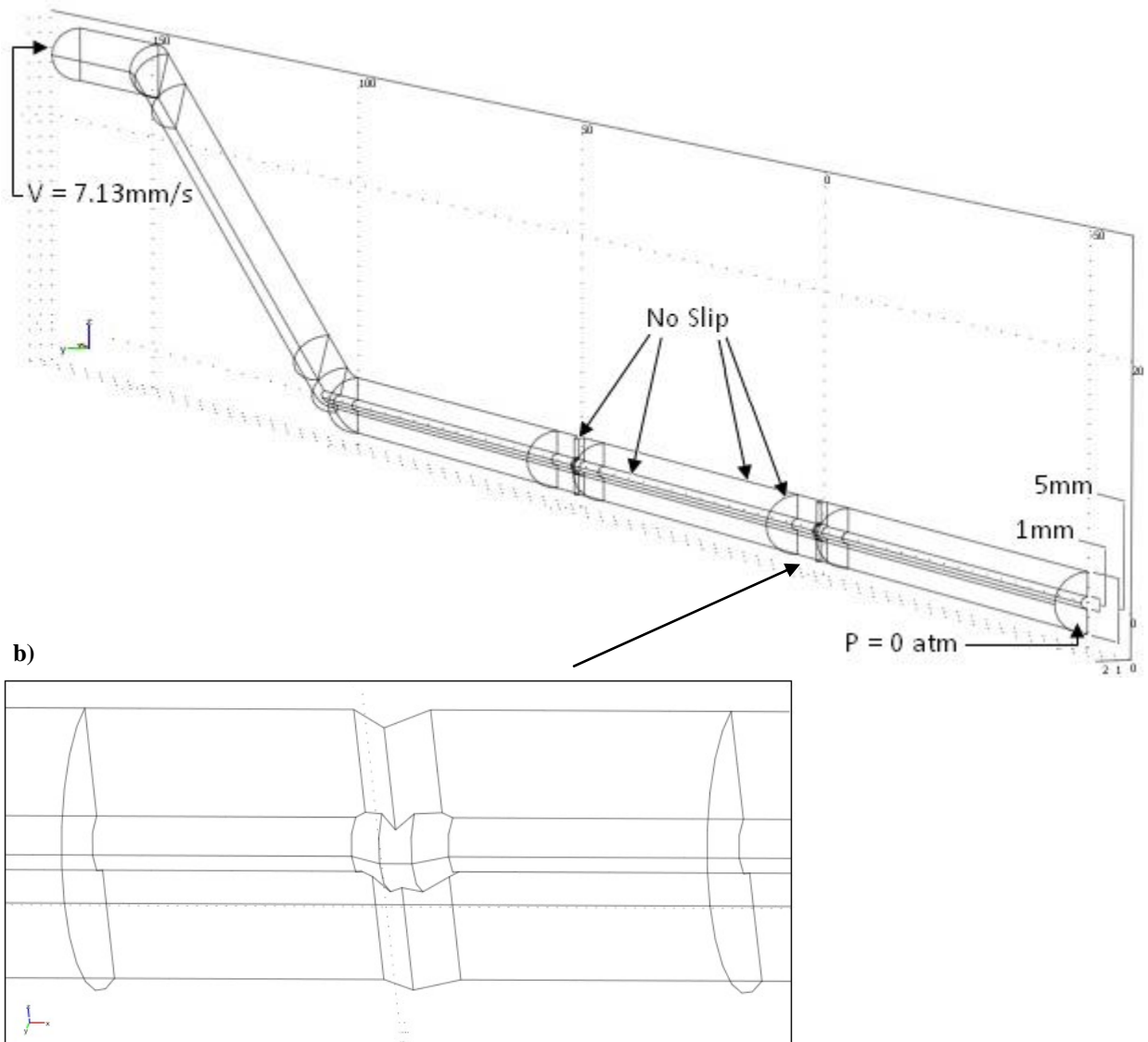


Figure 4. Schematic of simplified geometry used in COMSOL. (a) Due to symmetry, half of tube used for calculations. Inlet velocity is 7.13 mm/s, outlet pressure is considered to be atmospheric at 0 Pa. All walls, obstructions, and wire boundaries have no-slip boundary

condition while the boundary of the inside of the tube (due to modeling half) is symmetry (b) Enlarged depiction of supporting peg and guide wire running length of tube.

Results and Discussion

Qualitative Description of Process

The average inlet pressure was determined through boundary integration. Given the values presented in the Problem Schematic, the pressure at the input was calculated to be 380 kPa. In order to quantitatively assess this value, the units were converted to psi and multiplied by the cross-sectional area, resulting in a force value of 1.68 lbf. This amount of force is much less than the maximum force a single thumb can provide. The minimum measured maximum force for a male is over 10 lbf (Fig. 5). Thus it is reasonable to assume that the cement is free flowing down the tube and a physician could apply bone cement using the device without mechanical assistance.

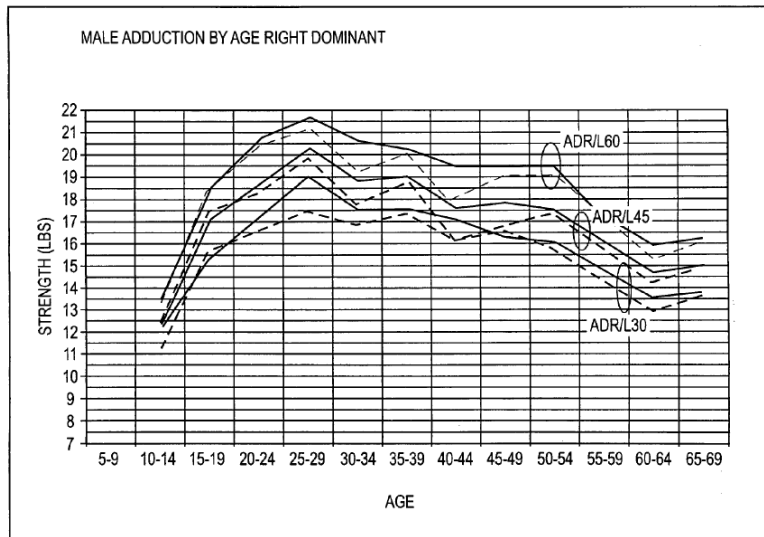


Figure 5. Male Thumb Adduction Strength as a Function of Age. Female thumb strength is less than males, but at comparable values well above the force necessary for the device to function.

Analyzing the pressure data over the length of the tube by sampling shows the specific nature of the pressure drops that occurred throughout the device (Fig. 6). In the first bend only a little pressure is lost. In the second bend there is also the addition of the central wire so there is a greater pressure loss due to increased friction of the wire and the bend. It is interesting to note that the rate of pressure drop is much greater in the section of the tube that has the wire than in the straight section. The points where there was the greatest pressure drops were in the obstructions. Looking at the derivative of the pressure change down the tube shows that the steepest decrease in pressure occurred in the sections surrounding the obstructions. Since the sampling sections were taken several millimeters before and after the obstruction, the pressure drop is not the effect of the Bernoulli relation of pressure and velocity.

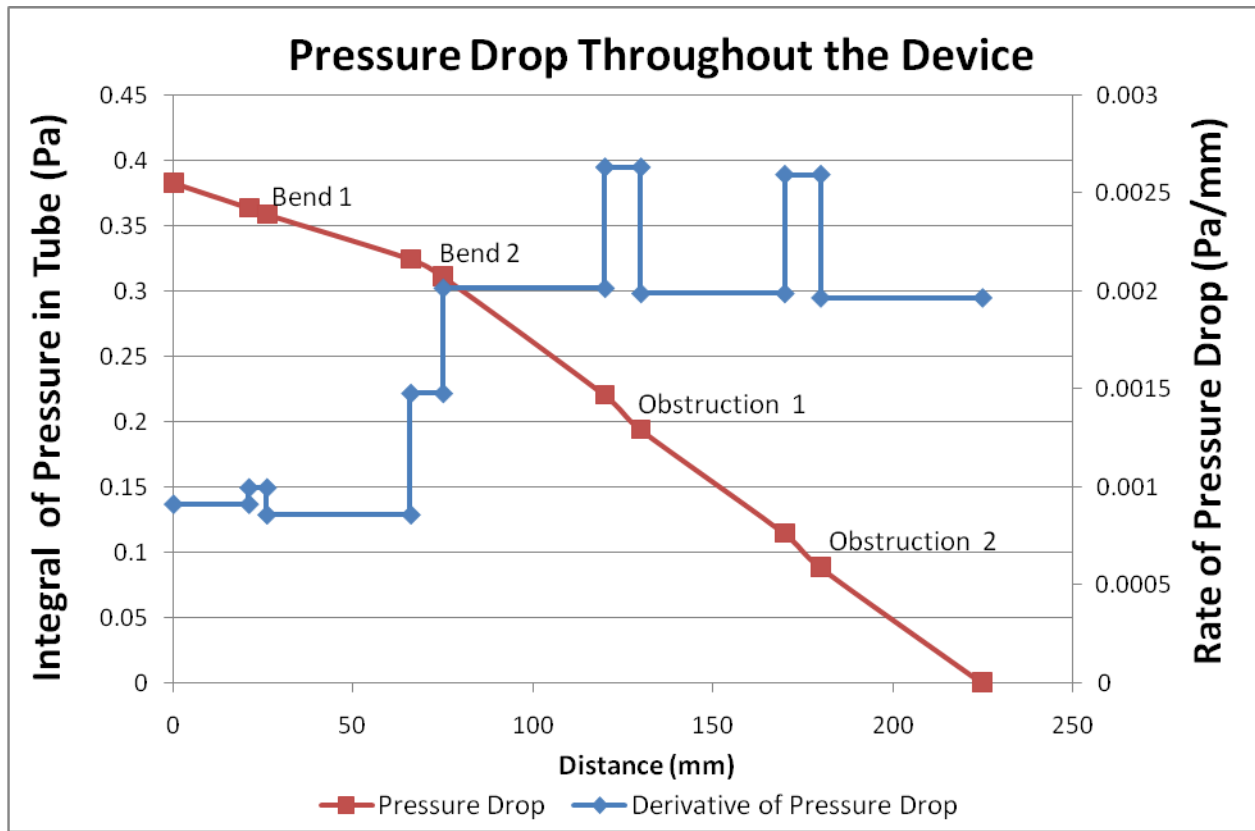


Figure 6. Pressure Drop Down Length of Tube. Sampled pressure values (red) by boundary integration at the boundaries between sub-domains. Rate of pressure drop (blue) was created using interpolation between pressure points.

Sensitivity Analysis

The parameters analyzed by sensitivity analysis were the PMMA viscosity and density as well as the inlet velocity. For each property, the x-velocity was determined by subdomain integration at the obstruction nearest the outlet; the percent change in these values is plotted against the percent change in the varying parameter, shown in Figure 7 below.

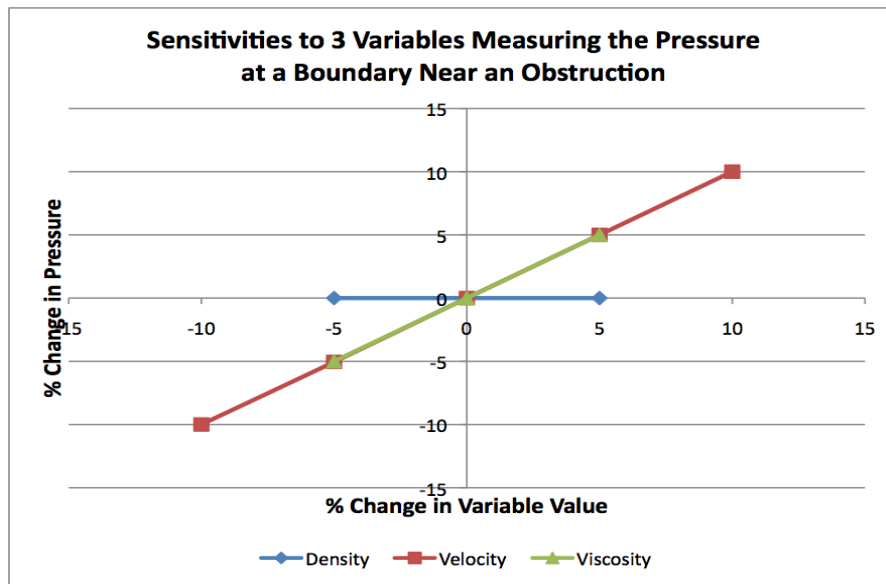


Figure 7. Sensitivity Analysis. Graph showing the relationships between three parameters (material density, material viscosity, and initial velocity) and the relative changes in pressure near a region of the tube near an obstruction.

PMMA viscosity was altered because in reality its viscosity changes with time as discussed previously with an example for Simplex-P formula in Figure 2. Thus, different values should be considered in the analysis to see if there would be any profound effects on the pressure within the tube as the time between the mixing of the PMMA components and the application through the tube is likely to vary within a range (before the onset of rapid curing) from surgery to surgery. We altered the viscosity by $\pm 5\%$ to determine if there are any significant changes to the profile in the tube. As shown in Figure 7, the resulting percent change in pressure is directly and proportionally related to the percent change in viscosity. In retrospect, there should be a much larger variation in these viscosities as shown by the value of the slope of the linearly increasing region of viscosity in Figure 2; up to 200%.

PMMA density also varies depending on factors such as the specific type and brand, mixing procedure, and storing conditions.^{7,8} The density value was changed by $\pm 5\%$ based on published values.^{7,8} Figure 7 shows the changing density had no effect on pressure..

As can be seen from Figure 7, there is no change in pressure near the obstruction with changes in density of the material. However, both viscosity and velocity drastically affect the pressure in the tube. They both have a linearly proportional relationship with the pressure, so if the viscosity increases by 5%, the pressure at the obstruction will increase by 5%. In the actual setup, the material is hardening with time, meaning the viscosity is increasing with time as well. The change in viscosity will cause the pressures in the tube to increase with time down its length. This means that surgeons must be very prepared before injection of the PMMA. The surgeon

must also be careful with how hard he or she pushes the material through the tube, as the increase in initial velocity will also increase the pressure at the same rate as viscosity. Further investigation is provided below.

The inlet velocity is perhaps the most important property to look at in the sensitivity analysis. This value will never be a constant, since a human surgeon will be applying the pressure to the end of the tube manually, thereby creating the inlet velocity. As can be seen in Figure 8, the amount of pressure the surgeon applies is directly related to the velocity with which PMMA will begin to travel down the tube.

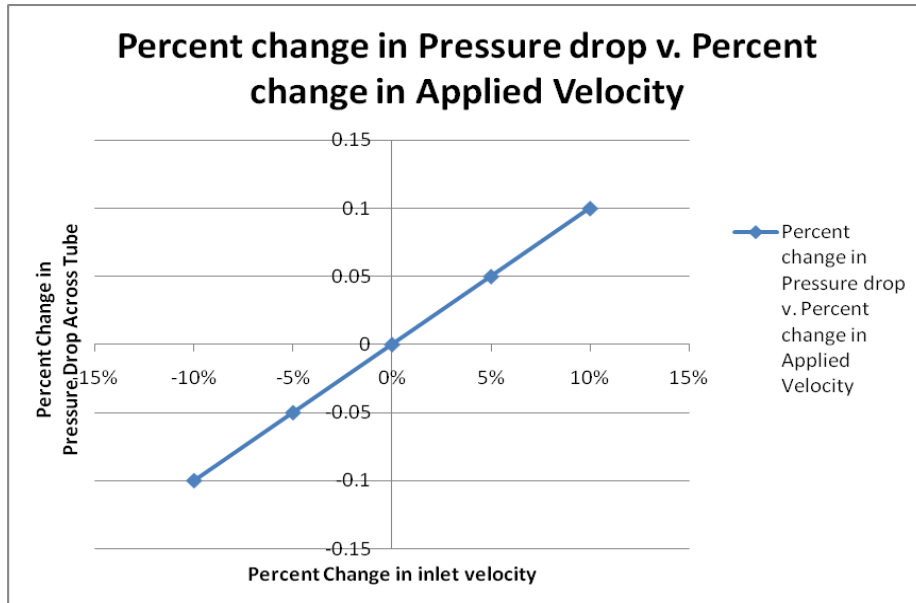


Figure 8. Effect of Applied Pressure on Initial Velocity. Connection between manually applied pressure and inlet velocity achieved. Direct relationship exists.

The inlet velocity was increased and decreased by 5% and 10%, since the varying surgical applied pressures were shown to directly affect these velocities. The effect on pressure at a point (boundary) near an obstruction is seen in Figure 7; however we are ultimately interested in the pressure drop throughout the entire setup. This was monitored by adjusting the inlet velocity in COMSOL and then measuring the pressure at the inlet boundary (since the outlet boundary is set at atmospheric pressure). The results can be seen in Figure 9 below. As with pressure at a point, pressure drop in the tube is directly linked to initial velocity values. It is again a direct relationship seen, with an increase of 5% in pressure drop attributed to a 5% increase in inlet velocity. The ensuing force that would need to be applied to create this 5% increase is approximately 1.81 lbf, which is still well below the magnitude that can be applied by a human.

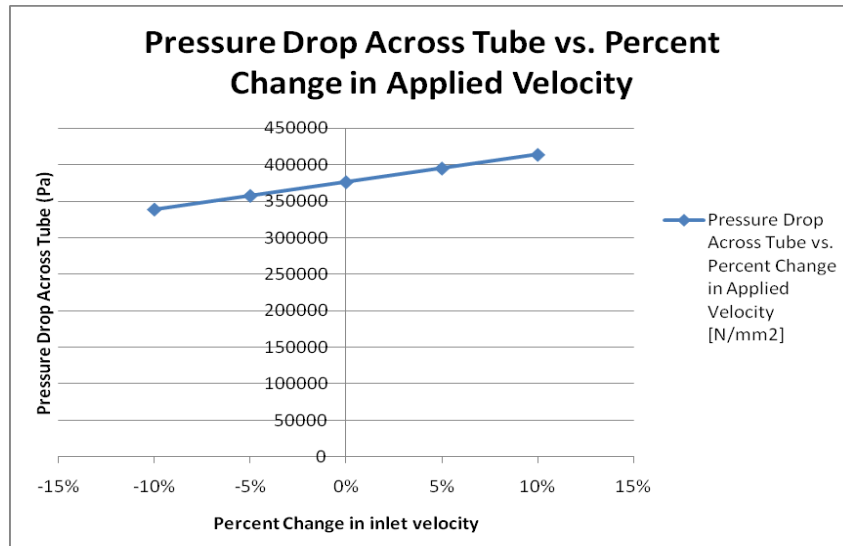


Figure 9. Pressure Drop as Affected by Inlet Velocity. Initial applied pressure was monitored to attain the pressure drop across entire pipe length with changing initial velocities.

Validation

To validate the computational model of the device a prototype of the device was made and tested using an instron 4502. For this test a prototype of the device was made using a styrene tube with an inner diameter of 3/16". A wire 1mm in diameter was inserted to run down the center of the tube starting at the second bend. Wires were inserted perpendicular to the wood backing at 50mm and 100mm from the bottom end of the wire to approximate the wire supports that exist in the device design. A syringe filled with bone cement was attached to the end to deliver bone cement down the tube as the instron head pushed against the syringe plunger. A head speed of 1.75mm/min was used to produce a velocity of 7.13mm/s down the tube. This rate was calculated from a syringe cross sectional area of 1935.32mm² and a tube cross sectional area of 78.54mm². The dry and wet components of bone cement were mixed quickly (~60sec) and put in the syringe before placing the entire apparatus under the instron



head. The graph produced was of load and displacement. The graph was converted using the head speed to a graph of force versus time. The tube was loaded with bone cement within the first 30 seconds and from then on it was at a steady state velocity with constant fluid flow through the tube. The change in force required to maintain the head speed was the result of the bone cement viscosity changing with time; hence the conversion of the data to force versus time.

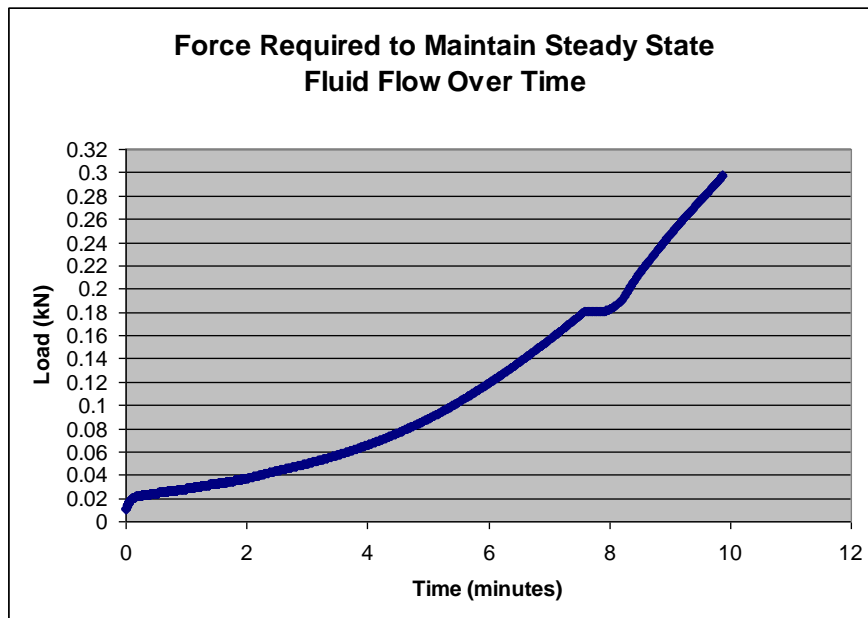


Figure 10 This is a plot of the force required to maintain a fluid velocity of 7.13mm/s. As time increases the viscosity of the bone cement increases which increases the pressure required to continue to move cement through the device.

Assuming the surgeon had a thumb strength of 17lbf, this converts to ~75 newtons. The force reaches 75N after 4.4 minutes. This means that a surgeon would have 4.4 minutes after they mixed and loaded the syringe to enter the nose and deposit the cement. This is well within the feasible range since a surgeon could reasonable deposit the cement in 30-60seconds.

Unfortunately the prototype does not match up with our model. This could be because the instron is also measuring the force from friction of the plunger in the syringe which was substantial and is shown in the plot by non-zero initial force. When this is factored out the prototype test would have reached the pressure of 380kPa from our model after 3.5 seconds. This indicates that the baseline viscosity we choose was too early in the formation of the cement since time was taken to mix the cement and load it to the syringe while it was curing. Since the cement can change viscosity by 200% in 30 seconds it is reasonable to assume that initial curing increases the viscosity of the fluid above our assumed value. Additionally we used Zimmer bone cement in the prototype and our model was based off of data from Simplex P bone cement which was not available for our tests. Although the values gathered were different from those we calculated in the model both the model and the prototype concur with our assertion that a surgeon could push bone cement through the device.

Conclusion and Design Recommendations

Review of Objectives

Starting out, this project aimed to complete an analysis of bone cement travel through a prototype biomedical device for use in skull base reconstructive surgeries. The difficulties observed were the viscous hardening nature of PMMA as well as the resistance in the tube caused by a central wire running down the length of the tube supported by supports acting as obstructions to fluid flow. The model discussed above simulates PMMA flow through a pipe with obstructions. While it is a simplified model, there is much to gain from these results. The value of initial pressure required to force the PMMA through the tube can most certainly be created from the force that is applied by a human surgeon's thumb. In fact, the force required is only about 20% of the force on the low end of the range of forces that can be applied by a human thumb. Therefore, a surgeon must be careful not to force the material through the device too quickly and inject too much PMMA. With greater computational power the pressure at the fluid inlet could be calculated at higher viscosities to model fluid flow later on in the curing process or model alternate brands of bone cement such as the one used in the prototype device. The low pressures calculated from the device and relatively comparable values in the prototype allow some flexibility in future designs of the wire and supports. The wire can be larger if needed to withstand greater turning force which may prove necessary for the device as a whole to operate. The supports can also be enlarged or their shape modified to stabilize the wire. The length of the tube can also be increased if it is found that the tube is not long enough to reach the back of the sinuses in larger patients. The calculated pressure is far enough below the maximum applicable pressures that there is substantial flexibility in the design constraints of future iterations of the device prototype.

Realistic Constraints

As with any real-life problem sought to be analyzed and solved by creating a model, there are realistic constraints to take into consideration when looking at the results obtained. Due to the nature by which a model is produced, not all variables are accounted for during experimentation. Simplifications of geometry and environmental conditions must be made to create the model, and these must not be forgotten when evaluating the results. Design constraints may also exist including economic, environmental, ethical, health safety, sustainability, and manufacturability.

In the case of this biomedical device the primary constraints of the model was the computational power available to run the model. With larger computers we could reduce simplifications and add extra parameters such a gravitational force. We would also be able to run the problem at high viscosities to create a plot of steady state flow as viscosity increases like the plot produced in validation.

Beyond the realm of the computational simulation of the device, the use of the device in the real world would require the device to go through testing, R&D, health and safety standards, marketing, all to get into the hands of surgeons to prove that the device improves patient health.

If any of these levels of development fall short, such as the logistics of finding funding, this device could never be constructed. This report sought to answer one of the realistic constraints of the device making it to market; whether at the end of the day it could be used. The answer from simulation and testing is yes and with considerable room for error. This device could be used by a surgeon with a single hand to seal skull base defects in humans.

Appendix A: Mathematical Statement of the Problem

Governing Equations

Our project is an analysis of the fluid flow of a non-Newtonian fluid, poly(methyl methacrylate), or PMMA. In order to be able to conduct this type of investigation using COMSOL, some simplification was necessary. We chose to model PMMA as an incompressible Newtonian fluid so that the Navier-Stokes equations could be utilized. They are presented here in Cartesian coordinates:

$$\begin{aligned}\rho \left(u \frac{\partial u}{\partial x} + v \frac{\partial u}{\partial y} + w \frac{\partial u}{\partial z} \right) &= -\frac{\partial p}{\partial x} + \mu \left(\frac{\partial^2 u}{\partial x^2} + \frac{\partial^2 u}{\partial y^2} + \frac{\partial^2 u}{\partial z^2} \right) \\ \rho \left(u \frac{\partial v}{\partial x} + v \frac{\partial v}{\partial y} + w \frac{\partial v}{\partial z} \right) &= -\frac{\partial p}{\partial y} + \mu \left(\frac{\partial^2 v}{\partial x^2} + \frac{\partial^2 v}{\partial y^2} + \frac{\partial^2 v}{\partial z^2} \right) \\ \rho \left(u \frac{\partial w}{\partial x} + v \frac{\partial w}{\partial y} + w \frac{\partial w}{\partial z} \right) &= -\frac{\partial p}{\partial z} + \mu \left(\frac{\partial^2 w}{\partial x^2} + \frac{\partial^2 w}{\partial y^2} + \frac{\partial^2 w}{\partial z^2} \right)\end{aligned}$$

where ρ is density (kg/m^3), u is velocity in the x-direction (m/s), v is velocity in the y-direction (m/s), w is velocity in the z-direction (m/s), p is pressure (Pa), μ is dynamic viscosity (Pa-s), and g_i is the gravitational constant in each respective direction (m/s^2 for $i = x, y, z$).

Boundary and Initial Conditions

- A velocity was specified as the inlet boundary condition:

$$u = 7.13 \text{ mm/s}$$

- Atmospheric pressure was assumed as the outlet boundary condition:

$$P = 0 \text{ (gauge)}$$

- A “no slip” boundary condition was used along all the walls of the tube, wire, and obstructions:

$$u = 0$$

Input Parameters

Table 1. Input Parameters. List of input parameters used and their reference sources.

Parameter	Symbol	Value	Source
Dynamic Viscosity	μ (η in COMSOL)	$1 \times 10^{-4} \frac{\text{N} \cdot \text{s}}{\text{mm}^2}$	1
Density	ρ	$1.10 \times 10^{-6} \frac{\text{kg}}{\text{mm}^3}$	2

Appendix B: Solution Strategy

Solver

The COMSOL Multiphysics 3.3 solver used in this project was the 3D Fluid Dynamics Incompressible Navier-Stokes Steady-state analysis.

Mesh

The mesh shown in Figure 10 was only used to compute a preliminary solution to show that our conditions would satisfy the physics known in fluid dynamics – no slip near boundaries and maximum velocity in the center of the tube. We created a rectangle dimensioned as 2 mm x 150 mm to simulate a cylinder with a solid wire representing the inner most boundary. To create a mesh that would be the finest at the surface of the cylinder and at the surface of the wire, we created a line in the middle of the rectangle so that we could have edge ratios going both directions from the center of the rectangle or the midpoint between the edge of the solid wire and the surface of the cylinder. This line had no properties nor did it take up any space so it did not affect the outcome of the solution. It was used solely for the purpose of creating a mapped mesh that would be coarse in the middle of the rectangle and finer on the edges.

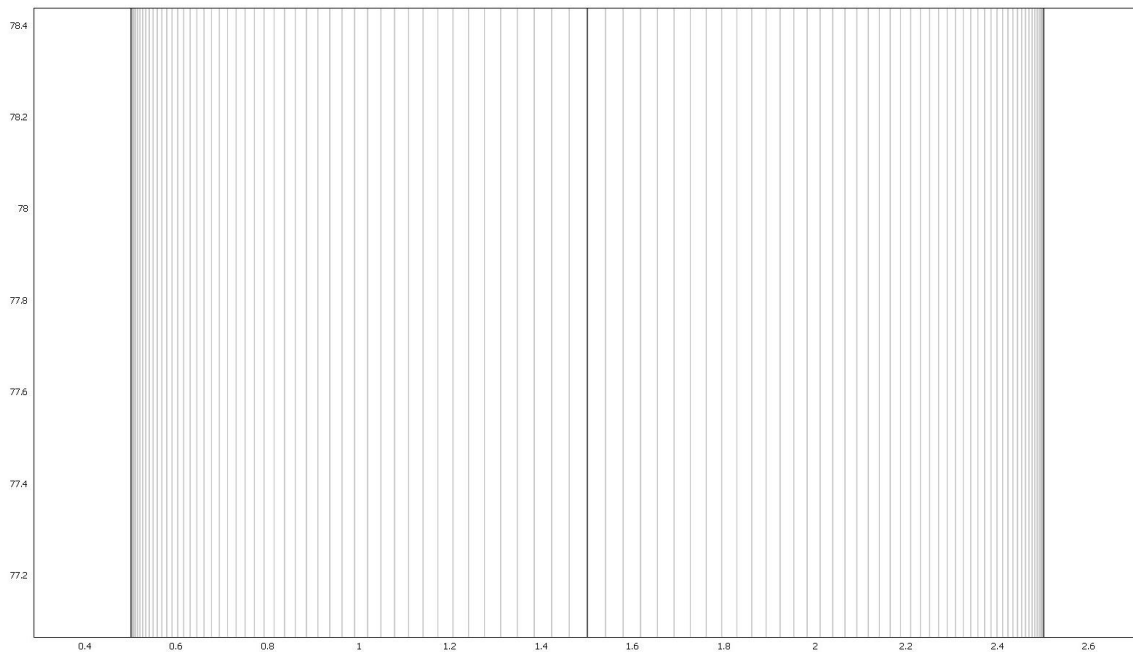


Figure 10. Preliminary 2D Mesh. Initial model created for use during preliminary analysis with axial symmetry around the center line (included for exploitation of edge ratios). Top view of the tube with the left boundary representing the edge of the center wire and the right boundary representing the edge of the tube.

We arrived at the final mesh shown in Figure 11 below through some trial and error between the sizing preferences in different regions of the tube (coarseness of mesh, growth ratio, etc). Two types of 3D elements were used in this mesh. A swept mesh was used in the straight sections of tube where no change in environment was present. These sections were generated using 8-node rectangular prisms. In the areas of interest – obstructions and bends – a free mesh of 4-node tetrahedral prisms was generated. Overall, the mesh near the boundaries was sought to be finer than the mesh in the center of the tube because the no slip boundary conditions present make the edges the starting points for changes in velocity.

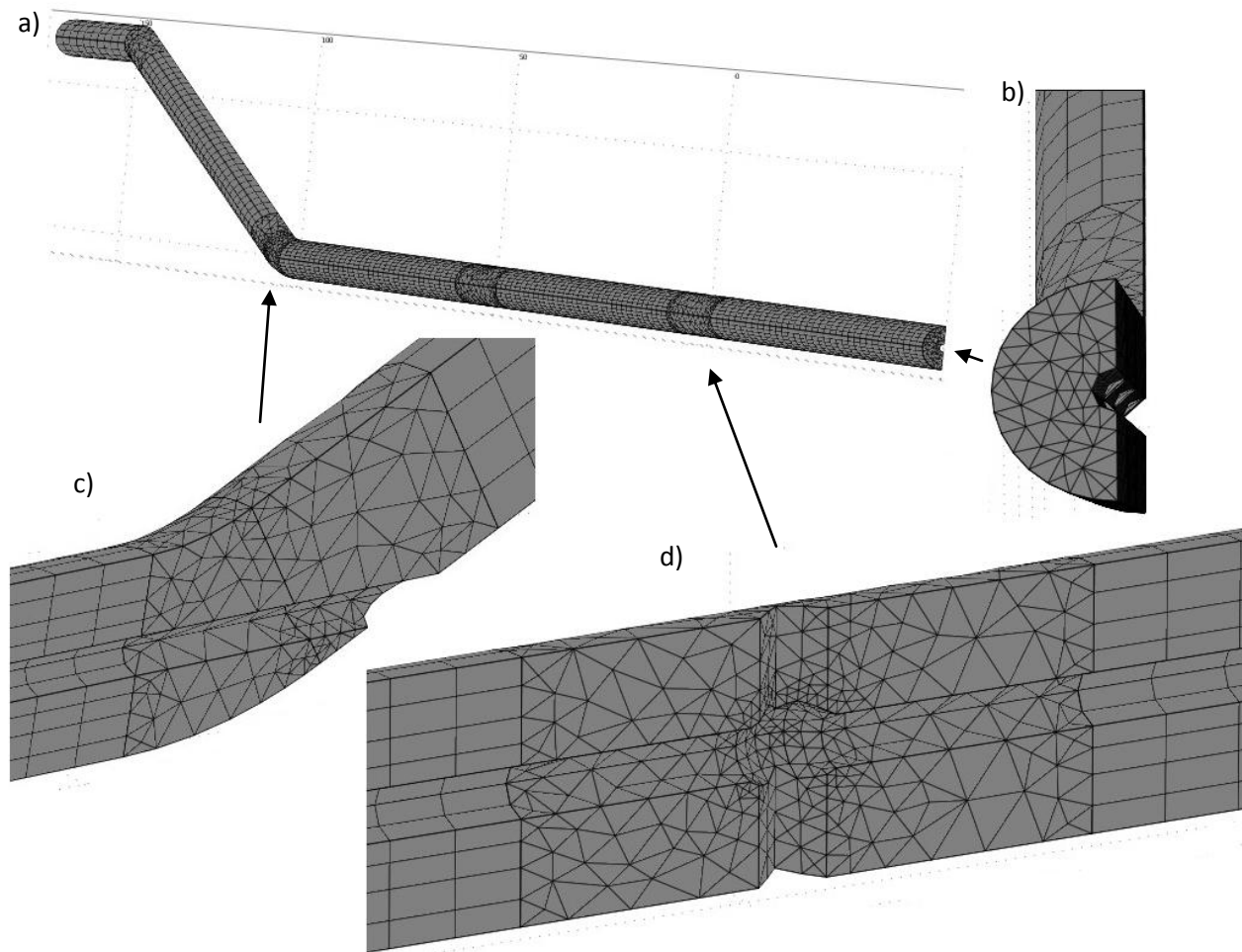


Figure 11. Final 3D Mesh. a) Full view of the mesh b) View of the outflow end of tube this free mesh is duplicated to create the swept mesh of the straight portions of the tube c) Free mesh at the second bend and the entry of the wire d) Free mesh of the area surrounding the obstruction

Mesh Convergence

A mesh convergence analysis was performed on the model. This was done by increasing the number of elements in the overall mesh while monitoring the velocity in the region containing the second obstruction (subdomain 2 of the structure). At first, only three meshes were used in the analysis, as can be seen represented by the three data points in Figure 12(a). The first mesh contained approximately 12,600 elements. It seemed as though convergence was obtained with our third mesh near 19,000 elements, however more validation of this assumption was necessary.

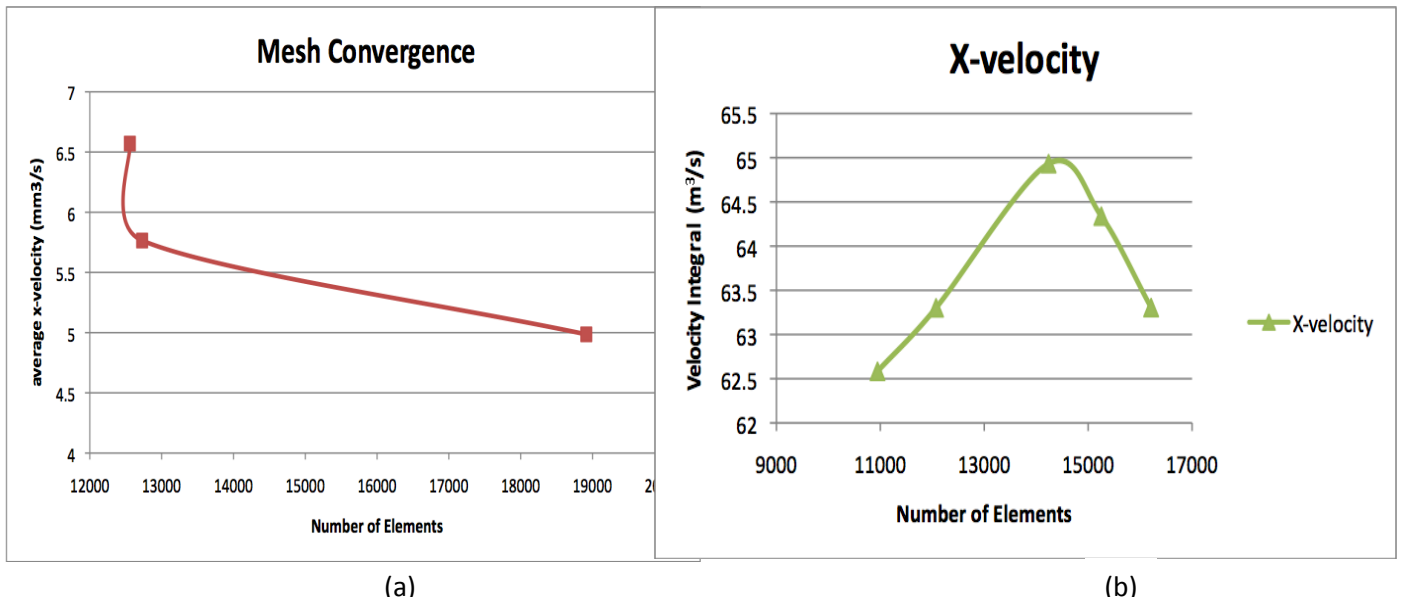
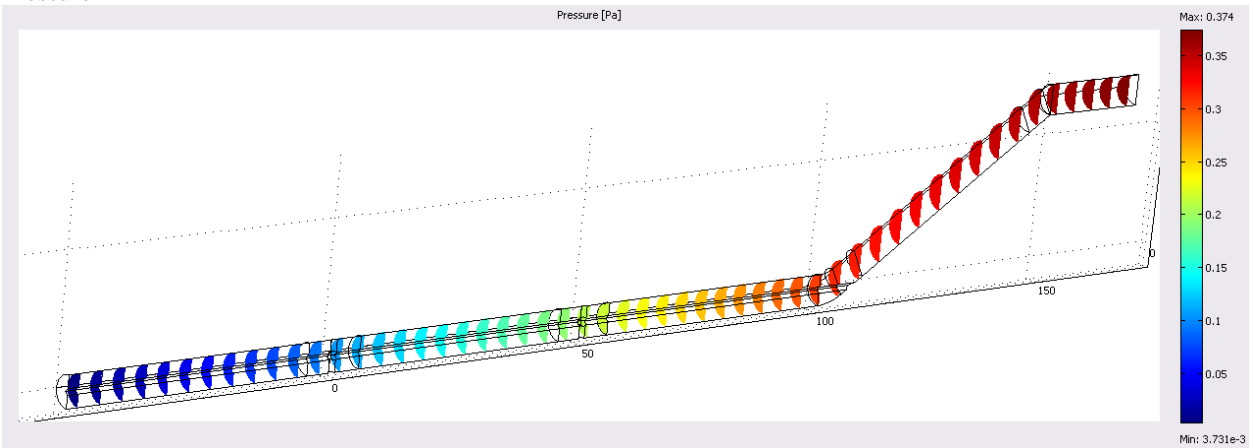


Figure 12. Mesh Convergence. Calculated using change in number of elements for entire structure versus the average x-velocity calculated for Subdomain 2, the final obstructed section (closest to exit) in the long horizontal portion of the pipe.

An additional mesh convergence was performed with new meshes, and the results can be seen in Figure 12(b). Starting with around 11,000 elements this time, the first two points seemed to give nonsense values as they had a prominently increasing slope. This can possibly be attributed to the meshes having too few elements for COMSOL to be accurate in its calculations. Looking at the chart in (a), the values between the ~12,600-element mesh and ~19,000-element mesh were accounted for in (b). Taking both plots into consideration, the meshes began to converge starting with the last point in (b), the final 16,000 element mesh. COMSOL's memory constraints prevented a solution with enough elements to show complete convergence.

Appendix C: Additional Visuals

Pressure



X-velocity

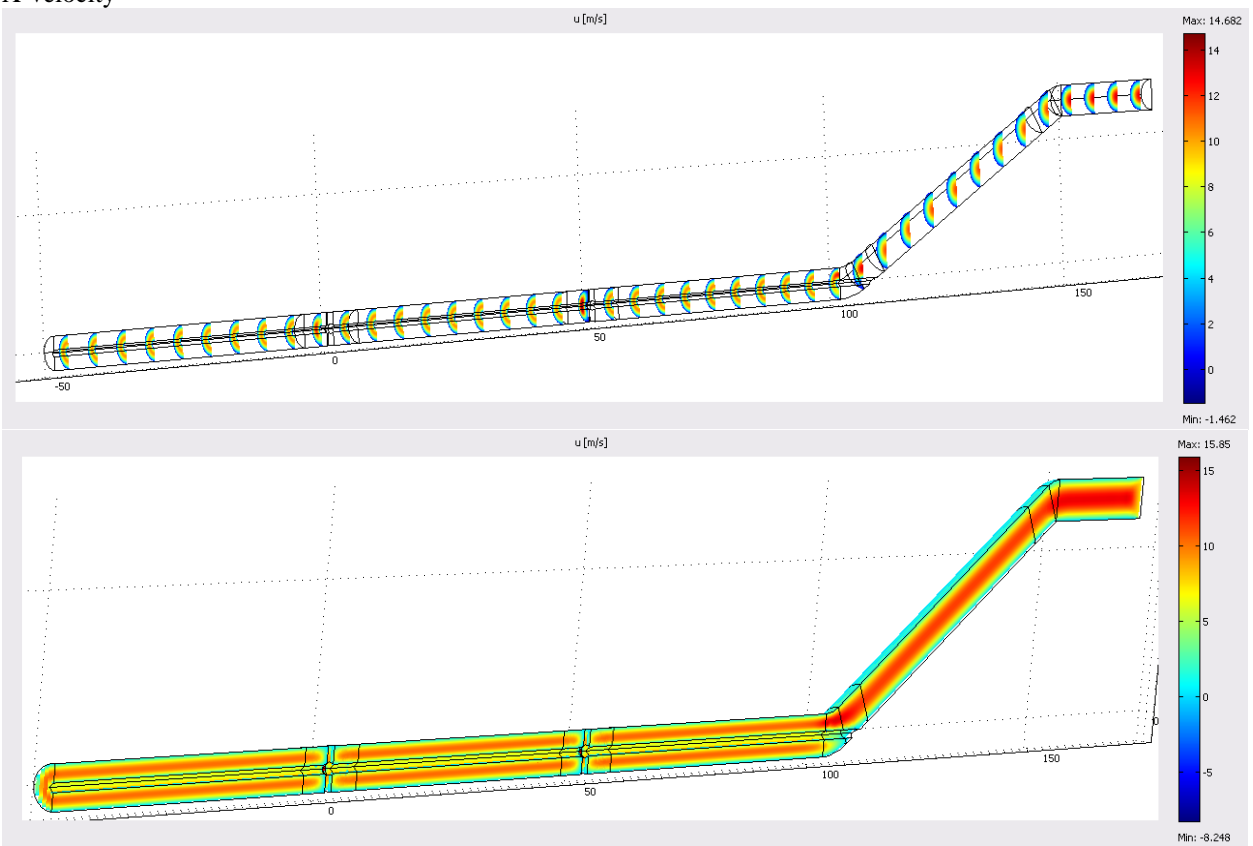


Figure 13. Velocity profiles and pressure drop over length of device.

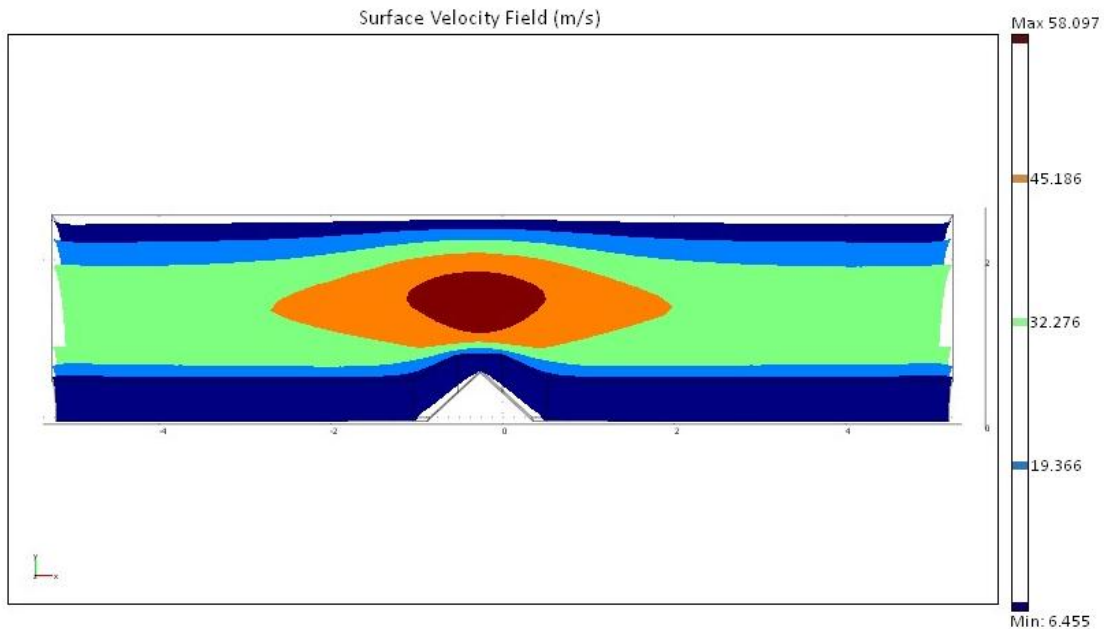


Figure 14. Velocity profile in device near a wire support. This figure shows how the velocity increases as the cross-sectional area of the pipe decreases as a result of the obstruction. The fluid is moving from right to left and there is a slight left skew of the velocity profile.

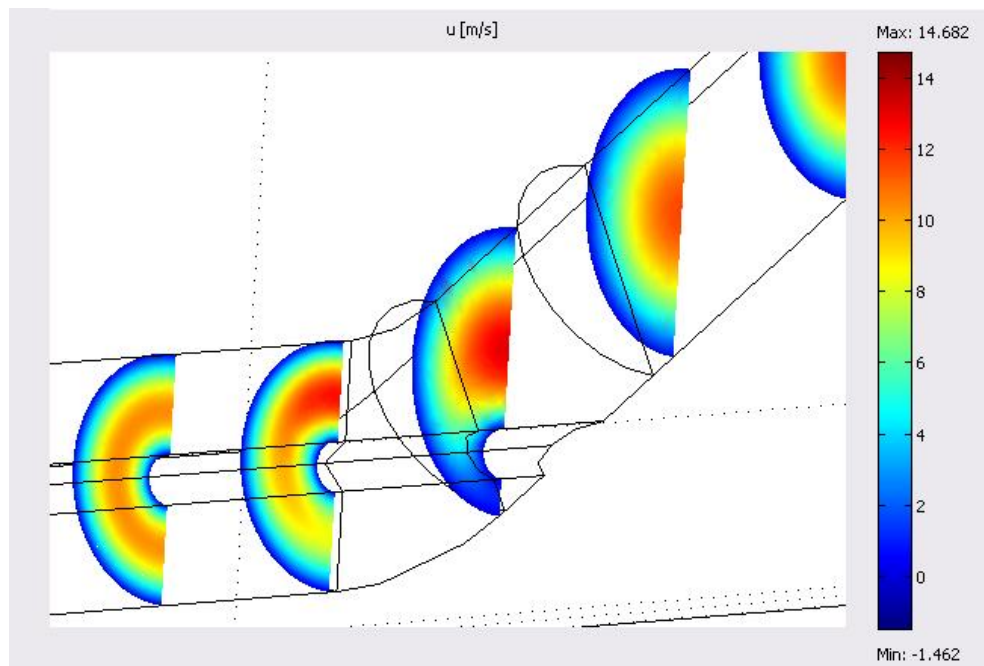


Figure 15. Velocity profile at bend of pipe and introduction of wire. This figure shows how the velocity profile behaves when contacting the wire. The wire blocks fluid flow so the lowest velocity is on the bottom. The wire is at an angle to the direction of fluid flow forcing the

majority of fluid through the inside of the curve which results in very high velocities but makes logical sense.

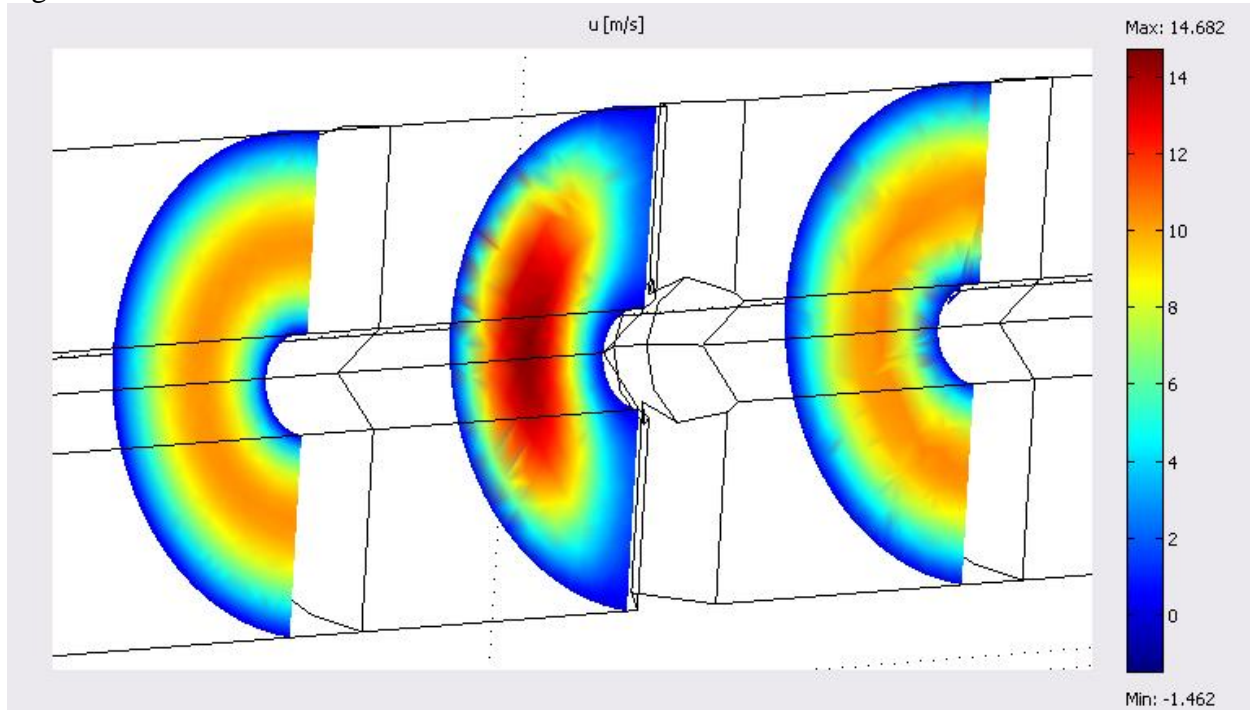


Figure 16. Another view of a velocity profile near a wire support. The velocity is the greatest between the inner and outer boundaries of the tube but slightly closer to the inner wire. Additionally the velocity profile near the obstruction is the greatest in the center of the space created by the tube wall and the obstruction. The obstruction creates a hemispherical section to the tube so the greatest velocity should be in the center. Note velocity moving in the negative direction.

References

1. Cavallo LM, MD, PhD; Messina A, MD; Cappabianca P, MD; Eposito F, MD; Divitiis E, MD; Gardner P, MD; Tschabitscher M, MD. "Endoscopic endonasal surgery of the midline skull base: anatomical study and clinical considerations." *Neurosurg Focus*. 19(1): E2, 2005.
2. Dean JR, Ison KT, Gishen P. "The Strengthening Effect of Percutaneous Vertebroplasty." *Clinical Radiology*. 55: 471-6, 2000.
3. Friedman JA., M.D.; Ebersold MJ, M.D.; Quast LM, R.N. "Post-traumatic Cerebrospinal Fluid Leakage." *World J. Surg.* 25: 1062–1066, 2001.
4. Jarrahy R, Cha ST, Berci G, Shahinian HK. "Endoscopic Transglabellar Approach to The Anterior Fossa and Paranasal Sinuses." *J Craniofacial Surgery* 11(5): 412-7, 2000.
5. Kabil, Mohamed S., MD, and Hrayr K. Shahinian, MD FACS. "Introduction to Endoscopic Skull Base Surgery." Powerpoint presentation. Skull Base Institute publications. <<http://www.skullbaseinstitute.com/papers.htm#research>>
6. Lian Z, Chui CK, SH Teoh. "A biomechanical model for real-time simulation of PMMA injection with haptics." *Computers in Biology and Medicine*. 38: 304-12, 2008.
7. Lewis, Gladius. "Properties of Acrylic Bone Cement: State of the Art Review." *J Biomed Mater Res*. 38: 155-182, 1997.
8. Lewis G, Nyman JS, Trieu HH. "Effect of Mixing Method on Selected Properties of Acrylic Bone Cement." *J. Biomed Mater Res*. 38(3): 221-8, 1997.
9. Rey RM Jr, B.A.; Paiement GD, MD; McGann WM, MD; Jasty M, MD; Harrigan TP, PhD; Burke DW, MD; and WH Harris, MD. "A Study of Intrusion Characteristics of Low Viscosity Cement Simplex-P and Palacos Cements in a Bovine Cancellous Bone Model." *Clinical Orthopaedics and Related Research*. 215: 272-8, 1987.
10. Rozmaryn, Leo M. US Patent 7127944 - System and method for measuring the motor strength of a human thumb or finger. Issued October 31, 2006.
11. Smeds S, MD, PhD; Goertzen D, MSc., Ivaarson Ingemar, MD, PhD. "Influence of Temperature and Vacuum Mixing on Bone Cement Properties." *Clinical Orthopaedics and Related Research*. 334: 326-33, 1997.
12. Serbetci K. and Nesrin Hasirci. 2003. Ch. 12: Recent Developments in Bone Cements. In: Biomaterials in Orthopedics by Yaszemski, MJ., Trantolo, DJ., Lewandrowski, K., Hasirci, V., Wise, DL., Altobelli, DE. (2nd ed.) Informa Health Care. p. 260.